Direct finite element method for nonlinear earthquake analysis of three-dimensional semi-unbounded dam–water–foundation rock systems

Arnkjell Løkke[1] and Anil K. Chopra[2]

[1] Department of Structural Engineering, Norwegian University of Science and Technology, 7491 Trondheim, Norway.

[2] Department of Civil and Environmental Engineering, University of California Berkeley, Berkeley, CA 94720, U.S.A.

DISCLAIMER

This is the pre-peer reviewed version of the following article: "Løkke, A., and Chopra, AK. (2018) Direct finite element method for nonlinear earthquake analysis of three-dimensional semi-unbounded dam–water–foundation rock systems. Earthquake Engineering and Structural Dynamics, 47: 1309–1328" which has been published in final form at Wiley Online Library [DOI: 10.1002/eqe.3019]. This article may be used for non-commercial purposes in accordance with Wiley Terms and Conditions for Self-Archiving.

SUMMARY

A direct finite element method for nonlinear earthquake analysis of two-dimensional dam–water–foundation rock systems has recently been presented. The analysis procedure uses standard viscous-damper absorbing boundaries to model the semi-unbounded foundation-rock and fluid domains, and specifies the seismic input as effective earthquake forces at these boundaries. Presented in this paper is a generalization of the direct finite element method with viscous-damper boundaries to three-dimensional dam-water-foundation rock systems. Step-by-step procedures for determining the effective earthquake forces starting from a ground motion specified at a control point on the foundation-rock surface is developed, and several numerical examples are computed and compared with independent benchmark solutions to demonstrate the effectiveness of the analysis procedure for modelling three-dimensional systems.

1. INTRODUCTION

Earthquake analysis of arch dams requires three-dimensional models of dam–water–foundation rock systems that recognize the factors known to significantly influence the earthquake response of concrete dams [1]: dam–water interaction including water compressibility and wave absorption in sediments deposited at the reservoir bottom [2]; dam–foundation rock interaction including mass, flexibility and damping in the rock [3,4]; radiation damping due to the semi-unbounded sizes of the reservoir and foundation-rock domains [3,5]; spatial variation of the ground motion at the dam–canyon interface [6,7]; nonlinear behavior of the dam and foundation rock [8–12].

Analysis procedures based on the *substructure method* [13–15] have long been available for linear frequency-domain analysis of three-dimensional dam–water–foundation rock systems. Most dam

engineers however, prefer to work with the *direct method* of analysis – implemented in commercial FE software with their user-friendly interfaces – that models the entire system using finite elements (FEs) and analyzes it directly in the time-domain. While these programs are able to model nonlinear mechanisms, they often neglect or use simplistic models for dam–water–foundation rock interaction and the semi-unbounded domains. Furthermore, the spatial variation of earthquake motions at the dam–canyon interface is typically ignored in dam engineering practice, although there is substantial evidence that such variations can significantly influence the response of arch dams [6,7].

Accurate modelling of dam–water–foundation rock systems by the direct method requires a FE model that includes the mass, stiffness, and material damping properties of the foundation rock, the compressibility of water, and the effects of sediments at the reservoir bottom. The semi-unbounded fluid and foundation-rock domains must be reduced to bounded sizes using *absorbing boundaries* [16,17], and the seismic input specified by *effective earthquake forces* applied directly to these boundaries [17,18], or alternatively, in a single layer of elements interior of the boundaries [19,20]. Utilizing the latter approach, Basu [21] developed an advanced analysis procedure using Perfectly Matched Layer (PML) [22] boundaries and the Effective Seismic Input method (ESI) [19] to specify effective earthquake forces. However, ESI and PML are features that require modification of the FE source code, and the procedure is currently only available in LS-DYNA [23].

Utilizing the former approach, a direct FE method for nonlinear earthquake analysis of two-dimensional dam–water–foundation rock systems has recently been presented [24]. Viscous-damper absorbing boundaries [25] were selected to model the semi-unbounded domains, and the effective earthquake forces were specified directly at these boundaries. These are standard features in FE analyses, thus ensuring that this direct FE method can be implemented with any commercial software without modification of the source code.

The objective of the work presented in this paper is to generalize the direct FE method with viscous-damper boundaries to three-dimensional dam–water–foundation rock systems. Step-by-step procedures for computing effective earthquake forces at the boundaries of the foundation-rock and fluid domains are presented, and several examples are documented to validate the accuracy of the analysis procedure applied to three-dimensional problems.

2. SYSTEM AND GROUND MOTION

2.1. Semi-unbounded dam–water–foundation rock system

The idealized, three-dimensional dam–water–foundation rock system considered consists of three subsystems (Fig. 1): (1) the concrete dam with nonlinear properties; (2) the foundation rock, consisting of a bounded region adjacent to the dam that may be nonlinear, inhomogeneous, and irregular in geometry; and the exterior, semi-unbounded, region with "regular" geometry that has linear constitutive properties and is homogeneous or horizontally layered; and (3) the fluid domain, consisting of a bounded region of arbitrary geometry adjacent to the dam that may be constitutively nonlinear; and a uniform channel, unbounded in the upstream direction, that is restricted to be linear.

By "regular" geometry of the semi-unbounded foundation-rock region we mean that the canyon upstream of the bounded region has a uniform cross-section, and similarly, the canyon downstream of the bounded region has a uniform cross-section; however, the two cross-sections may be different. The assumption of homogeneous or horizontally layered properties in the exterior foundation-rock region is introduced to permit use of a deconvolution method to define the seismic input for the system starting from a ground motion specified at the surface of the foundation rock (Sec. 2.2).

The semi-unbounded system in Fig. 1 is modeled by a three-dimensional FE discretization of a bounded system with wave-absorbing boundaries at the bottom and side boundaries of the foundation-rock domain to model its semi-unbounded geometry, and at the upstream end of the fluid domain to

model its essentially "unbounded" length (Fig. 2). Although many absorbing boundaries have been proposed in the literature, the well-known viscous damper [25] is chosen herein because of its availability in almost every commercial FE code, acceptable accuracy, and ease of implementation.

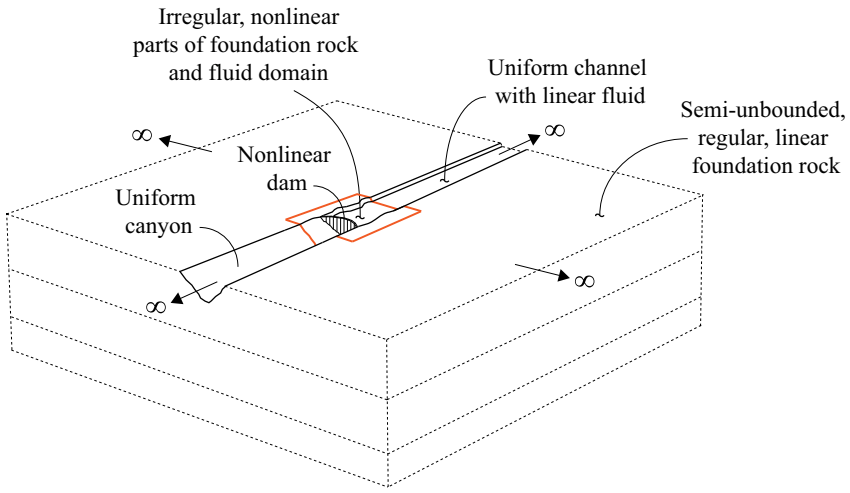

Figure 1: Three-dimensional semi-unbounded dam–water–foundation rock system showing three subsystems: (1) the nonlinear dam; (2) the foundation rock, consisting of an irregular, nonlinear region and a semi-unbounded linear region with "regular" geometry and properties; (3) the fluid domain, consisting of an irregular (possibly nonlinear) region, and a semi-unbounded uniform channel with linear fluid.

The linear, regular parts of the foundation-rock and fluid domains included in the FE model (Fig. 2) provide a transition from the irregular geometry and nonlinear behavior adjacent to the dam to the regular geometry and linear behavior required at the absorbing boundaries. The minimum sizes for these domains are determined by the ability of the viscous-damper boundaries to absorb outgoing (scattered) waves from the system. Because the viscous damper is a "simple" absorbing boundary, larger domain sizes are required than if an "advanced" boundary such as PML was used.

The use of finite elements for the entire system permits modeling of arbitrary geometry and inhomogeneous, nonlinear material properties of the dam, canyon, and foundation-rock and fluid domains adjacent to the dam. Furthermore, it allows for modelling of nonlinear mechanisms such as cracking of the dam concrete, sliding and separation at construction joints, lift joints, and at concrete–rock interfaces, discontinuities in the rock due to local cracks and fissures, and cavitation in the fluid.

2.2. Earthquake excitation

Equations governing the response of the system of Fig. 2 subjected to earthquake excitation defined by the "free-field" ground motion – the motion that would occur in the foundation rock without the dam and water present – will be formulated in Sec. 3. These equations require that the spatially varying free-field motions at all boundaries of the FE model are known. Specifying such motions remains a challenging problem.

The most general approach is to perform large-scale simulation of seismic wave propagation from an earthquake source to the dam site, shown schematically in Fig. 3a. Here, physics-based finite element or finite difference models of large 3D regions subjected to a fault slip are analyzed. Although such regional simulations have been reported in the research literature [26,27], they seem impractical for concrete dam analyses for two reasons: (1) information regarding the details of the earthquake fault

rupture and properties of the geological materials is lacking; and (2) simulation models are currently limited to lower frequencies compared to the vibration properties of concrete dams.

Another approach would be to use boundary element methods (BEM) to compute the free-field motions resulting from incident plane waves propagating from infinity to the dam site at predefined angles, shown schematically in Fig. 3b. Such methods have been used to compute the free-field motions at the surface of canyons and to investigate the influence of assumed incident angles on the dam response [7,28]. However, due to the obvious difficulty in selecting a combination of wave types and their incidence angles for an actual situation, these methods are rarely applied to solve practical problems.

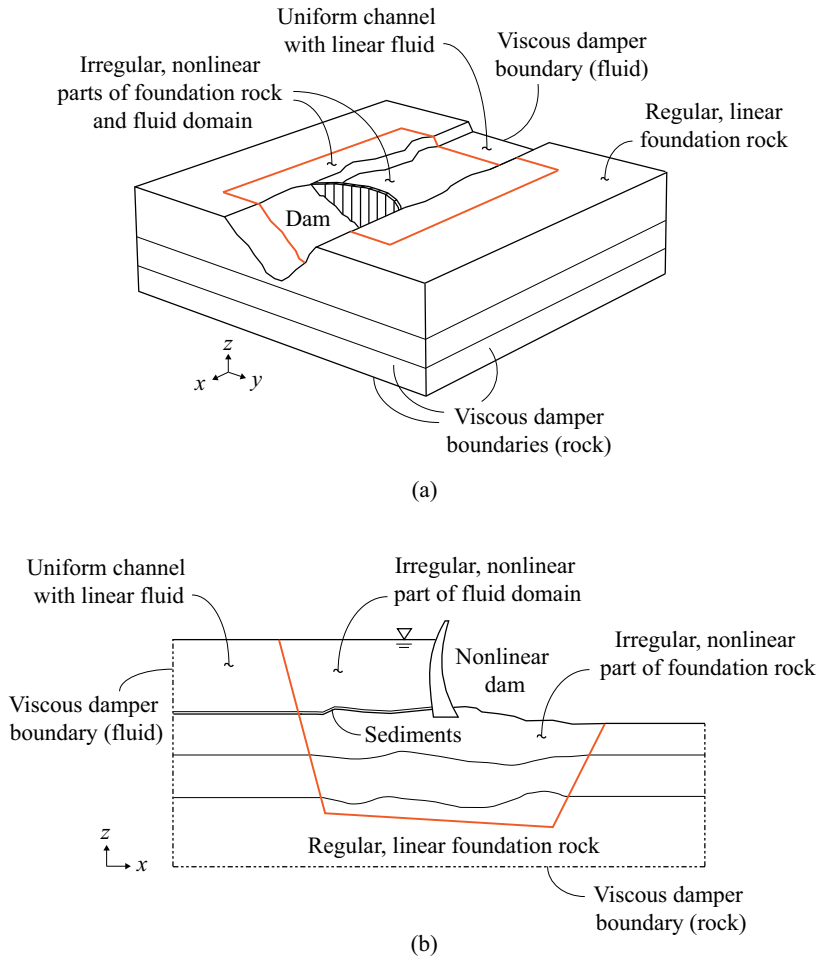

Figure 2: Dam–water–foundation rock system with truncated foundation-rock and fluid domains: (a) 3D perspective view; (b) section view through center of canyon.

Presently, the standard approach is to define the earthquake excitation by three components of free-field acceleration at a control point on the foundation-rock surface (Fig. 3c): the stream component, $a_g^x(t)$, the cross-stream component $a_g^y(t)$ and the vertical component $a_g^z(t)$. Because the ground motion cannot be defined uniquely, we are interested in an ensemble of motions. These should, in some sense, be consistent with a target spectrum that represents the seismic hazard at the site, e.g., the uniform hazard spectrum (UHS) or some variation of the conditional mean spectrum (CMS). Several methods have been developed to select and scale ground motion records to "match" a target spectrum [29]. The UHS (and

CMS) applies to an outcrop location on level ground; this control point is usually chosen at the elevation of the dam abutments. It could also be at other locations however, for example if the purpose is to perform analysis using earthquake input motions recorded at specific locations near the dam.

The free-field motion at the bottom and side boundaries of the foundation-rock domain can be determined from the surface control motion $a_g(t)$ using a deconvolution-type analysis (Fig. 3c). For this analysis, it will be assumed that the incident wave field consists solely of plane *SH*-, *SV*- and *P*-waves propagating vertically upwards from the underlying semi-unbounded foundation rock. This is clearly a major simplification, but at the present time, it seems to be a reasonable pragmatic choice.

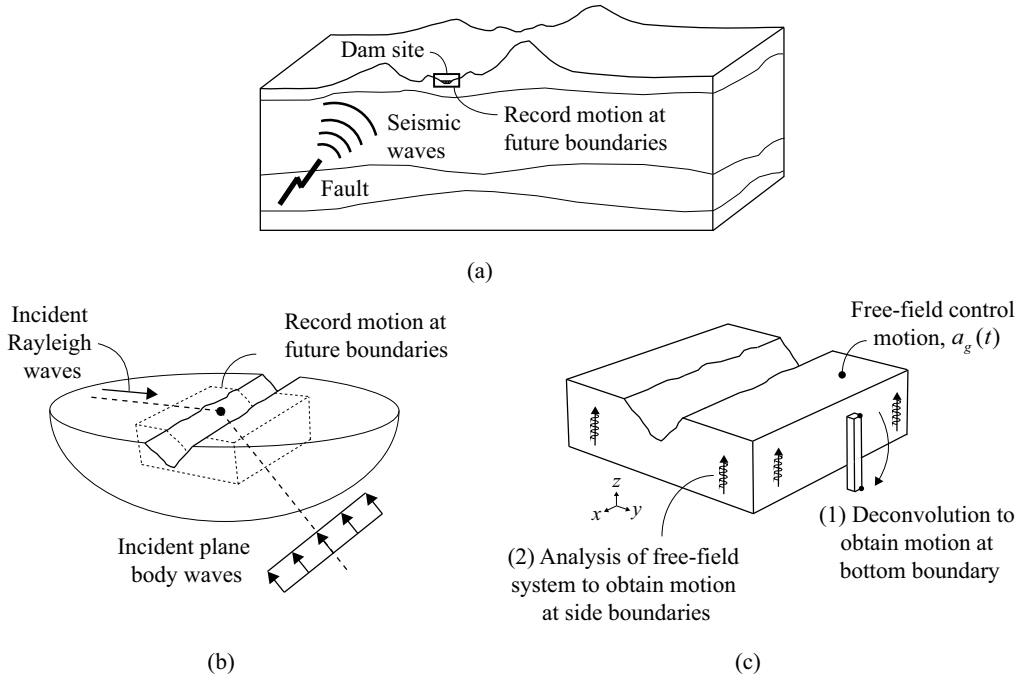

Figure 3: Schematic overview of methods to obtain free-field earthquake motion: (a) large scale fault-rupture simulation; (b) boundary element method with incident plane waves propagating from infinity at predefined angles; (c) deconvolution analysis starting with a free-field surface control motion $a_g(t)$.

When specifying the earthquake excitation this way, spatial variation of the ground motion, both amplitude and phase, is automatically considered in the analysis. Variations in the vertical direction arise from wave propagation effects, and scattering and diffraction of waves from the canyon cause variation in the horizontal direction. Because of the simplifying assumption of vertically propagating incident waves, this spatial variation is significant in the vertical direction, but less so in the horizontal direction.

3. EQUATIONS OF MOTION

The equations governing a two-dimensional dam–water–foundation rock system idealized as an ensemble of finite elements with viscous-damper absorbing boundaries were derived in [24] by interpreting dam–water–foundation rock interaction as a scattering problem in which the dam perturbs the "free-field" motion in an auxiliary state of the system. The resulting equations of motion have recently been generalized to three-dimensional dam–water–foundation rock systems [30]. Presented here without derivation, the final equations of motion for the FE system (Fig. 4) are:

$$\begin{bmatrix} \mathbf{m} & \mathbf{0} \\ \rho(\mathbf{Q}_h^{\mathrm{T}} + \mathbf{Q}_b^{\mathrm{T}}) & \mathbf{s} \end{bmatrix} \begin{Bmatrix} \ddot{\mathbf{r}}^t \\ \ddot{\mathbf{p}}^t \end{Bmatrix} + \begin{bmatrix} \mathbf{c} + \mathbf{c}_f & \mathbf{0} \\ \mathbf{0} & \mathbf{b} + \mathbf{c}_r \end{bmatrix} \begin{Bmatrix} \dot{\mathbf{r}}^t \\ \dot{\mathbf{p}}^t \end{Bmatrix} + \begin{Bmatrix} \mathbf{f}(\mathbf{r}^t) \\ \mathbf{0} \end{Bmatrix} + \begin{bmatrix} \mathbf{0} & -(\mathbf{Q}_h + \mathbf{Q}_b) \\ \mathbf{0} & \mathbf{h} \end{bmatrix} \begin{Bmatrix} \mathbf{r}^t \\ \mathbf{p}^t \end{Bmatrix} = \begin{Bmatrix} \mathbf{R}^{\mathrm{st}} \\ \mathbf{0} \end{Bmatrix} + \begin{Bmatrix} \mathbf{P}_f^0 \\ \mathbf{P}_r^0 \end{Bmatrix} \tag{1}$$

where $\mathbf{r}^t$ is the vector of total displacements in the dam and foundation rock; $\mathbf{p}^t$ is the vector of total hydrodynamic pressures in the fluid idealized as a linear*, inviscid, irrotational and compressible acoustic fluid; $\mathbf{m}$ and $\mathbf{c}$ are the standard mass and damping matrices, respectively, for the dam–foundation rock system; $\mathbf{f}(\mathbf{r}^t)$ is the vector of internal forces due to (nonlinear) material response; $\mathbf{s}$, $\mathbf{b}$ and $\mathbf{h}$ are the "mass", "damping" and "stiffness" matrices for the acoustic fluid [31], respectively; $\mathbf{c}_f$ is the matrix of normal and tangential damper coefficients for the viscous dampers (dashpots) on the foundation-rock boundaries Γ_f; $\mathbf{c}_r$ is the matrix of damper coefficients for the viscous dampers on the upstream fluid boundary Γ_r; ρ is the density of water; $\mathbf{Q}_h$ and $\mathbf{Q}_b$ are matrices that couple accelerations to hydrodynamic pressures at the dam–water interface Γ_h and water–foundation rock interface Γ_b, respectively; $\mathbf{R}^{\mathrm{st}}$ is the vector of static forces that includes self-weight, hydrostatic pressures, and static foundation-rock reactions at Γ_f.

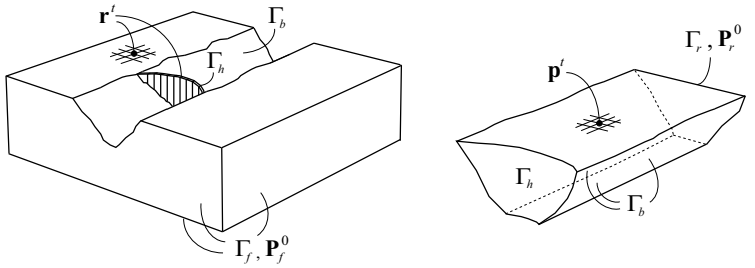

(a) (b)

Figure 4: Schematic overview of FE model of (a) dam and foundation-rock domain, (b) fluid domain. Highlighted are the viscous damper boundaries Γ_f and Γ_r at the truncation of the foundation-rock and fluid domains, and the fluid-solid interfaces Γ_h at the upstream dam face and Γ_b at the reservoir bottom and sides.

Hydrodynamic wave energy is lost at Γ_b – the bottom and side boundaries of the reservoir – by means of two different mechanisms. The first is wave absorption in sediments deposited at the reservoir bottom. This mechanism is modeled by the reservoir bottom reflection coefficient α [32], and its effects are included in Eq. (1) through the damping matrix $\mathbf{b}$. The second mechanism, associated with water–foundation rock interaction, is explicitly considered in the FE model through the coupling matrix $\mathbf{Q}_b$. Because this mechanism automatically accounts for some radiation of hydrodynamic waves, care should be taken not to overestimate the total amount of energy lost at these boundaries when also including sediment absorption in the FE model.

The earthquake excitation is specified in Eq. (1) by the effective earthquake forces $\mathbf{P}_f^0$ and $\mathbf{P}_r^0$ [30]:

* For convenience of notation, the fluid is assumed to be linear also in the irregular fluid part. The resulting formulation is applicable to nonlinear fluids in the irregular fluid part with appropriate generalization [49].

$$\mathbf{P}_f^0 = \mathbf{R}_f^0 + \mathbf{c}_f \dot{\mathbf{r}}_f^0 \text{ at the foundation-rock boundaries } \Gamma_f \tag{2a}$$

$$\mathbf{P}_r^0 = \mathbf{c}_r \dot{\mathbf{p}}_r^0 \text{ at the upstream fluid boundary } \Gamma_r \tag{2b}$$

where the *free-field motion* $\mathbf{r}_f^0$ and *free-field boundary forces* $\mathbf{R}_f^0$ at Γ_f are to be computed from analysis of the free-field foundation rock, defined as the foundation-rock domain without the dam and reservoir (Fig. 5a); and the *free-field hydrodynamic pressures* $\mathbf{p}_r^0$ at Γ_r are to be computed from analysis of the free-field fluid domain, defined as the uniform channel upstream of Γ_r (Fig. 5b).

The free-field variables $\mathbf{r}_f^0$, $\mathbf{R}_f^0$ and $\mathbf{p}_r^0$ represent the minimal set of data required to determine the response of the dam–water–foundation rock system to earthquake excitation. Procedures for computing these variables at the different boundaries will be presented next in Sec. 4.

4. COMPUTING EFFECTIVE EARTHQUAKE FORCES

4.1. Forces at bottom boundary of foundation-rock domain

To facilitate implementation of the procedure, it is convenient to reformulate Eq. (2a) for the effective earthquake forces at the bottom foundation-rock boundary [30]:

$$\mathbf{P}_f^0 = 2\mathbf{c}_f \dot{\mathbf{r}}_I^0 \tag{3}$$

where $\mathbf{r}_I^0$ is the motion at the bottom boundary associated with the incident (upward propagating) seismic waves. Because this equation only requires the incident motion $\mathbf{r}_I^0$, it avoids computation of the free-field boundary tractions $\mathbf{R}_f^0$ that are required when using Eq. (2a) directly.

The incident motion $\mathbf{r}_I^0$ is obtained by 1D deconvolution of the surface motion $a_g(t)$ assuming vertically propagating seismic waves and a homogeneous (or horizontally layered) rock halfspace (Fig. 3c). Deconvolution is an inverse procedure to determine the amplitude and frequency content of an input signal to be consistent with the observed output signal. It is most conveniently implemented in the frequency domain, either directly by computing the transfer function for a 1D halfspace, or by utilizing 1D wave propagation software such as SHAKE [33] or DEEPSOIL [34].

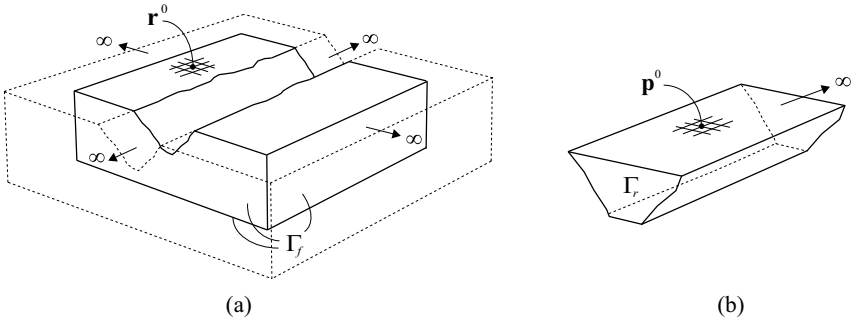

Figure 5: (a) Free-field foundation rock system (without dam or reservoir) with displacements defined by $\mathbf{r}^0$, (b) "free-field" fluid channel upstream of Γ_r with hydrodynamic pressures defined by $\mathbf{p}^0$.

Although rather straightforward, deconvolution is often subject to considerable confusion because 1D wave propagation software operate with two possible motions at every depth [35]: an *outcrop motion* and a *within motion*. By definition, the within motion is the superposition of the incident and reflected

waves, i.e., it is the total (or "actual") motion at any given depth in the halfspace. In contrast, the outcrop motion is the motion that would occur at a theoretical outcrop location at the same depth; this is equal to twice the amplitude of the incident motion. Thus, the incident motion $\mathbf{r}_I^0$ needed in Eq. (3) is one-half the outcrop motion at the bottom boundary determined from the deconvolution analysis. The procedure to compute effective earthquake forces $\mathbf{P}_f^0$ from Eq. (3) is summarized in Box A1 in Appendix A.

Some researchers have avoided deconvolution of the surface motion by idealizing the foundation rock as a homogeneous, undamped halfspace [5,36]. In this special case, a vertically propagating wave does not attenuate, implying that the incident motion $\mathbf{r}_I^0$ at the bottom boundary is equal to one-half the surface control motion, except for a time shift. While this simplification may be appropriate for some cases (rock with high stiffness and very little inherent material damping), it does not appear to be always valid.

4.2. Forces at side boundaries of foundation-rock domain

4.2.1. Free-field boundary elements

The computation and application of effective earthquake forces at the four side boundaries of the foundation-rock domain (Eq. 2a) can be performed automatically within the FE code using a special class of free-field boundary elements [37]. These elements solve the radiation condition for one-dimensional wave propagation and apply consistent forces at the boundaries at every time step as the analysis progresses in time. However, only a very few commercial programs have such boundary elements available for three-dimensional analysis, examples are PLAXIS [38] and FLAC [39].

In light of the limited availability of these elements, we will present an alternative procedure wherein the effective earthquake forces are computed in a separate auxiliary analysis of the free-field system before the actual dam–water–foundation rock system is analyzed. This approach has the advantage that it does not require modification of the FE source code, but has the disadvantage that it requires major data transfer.

4.2.2. Computing $\mathbf{P}_f^0$ at side boundaries

The free-field motion $\mathbf{r}_f^0$ and boundary forces $\mathbf{R}_f^0$ required to compute the effective earthquake forces $\mathbf{P}_f^0$ at the four side boundaries of the foundation-rock domain from Eq. 2a are to be determined from dynamic analysis of the foundation-rock in its free-field state (Fig. 5a). Although this system is much simpler than the actual dam–water–foundation rock system, it is still too complicated to analyze directly by the direct FE method because it contains the irregular canyon interior of the boundary Γ_f.

The quantities $\dot{\mathbf{r}}_f^0$ and $\mathbf{R}_f^0$ that enter in Eq. (2a) can instead be determined for each component of ground motion from two sets of four simpler analyses [30]: (i) four 1D corner columns subjected to forces of Eq. (3) at the base are analyzed first to provide $\dot{\mathbf{r}}_f^0$ and $\mathbf{R}_f^0$ for the corner nodes; (ii) analyses of four 2D systems subjected to forces of Eq. (3) at its base and forces $\mathbf{P}_f^0$ on the sides determined from the first set of 1D analyses (required because the domain has been truncated) provides $\dot{\mathbf{r}}_f^0$ and $\mathbf{R}_f^0$ for nodes on all four side boundaries. The procedure is illustrated in Fig. 6 and summarized in step-by-step form in Box A2 in Appendix A.

This procedure for computing $\mathbf{P}_f^0$ at the side boundaries of a system with arbitrary geometry is based on the assumption that the motion in each of the four 2D systems in Fig. 6a can be determined independently of the other 2D systems. This assumption is reasonable as long as the foundation-rock domain is large enough, which is generally the case because the viscous-damper boundaries already require large domains to ensure acceptable modeling of the semi-unbounded domains. A more detailed discussion on the significance of this assumption can be found in [30].

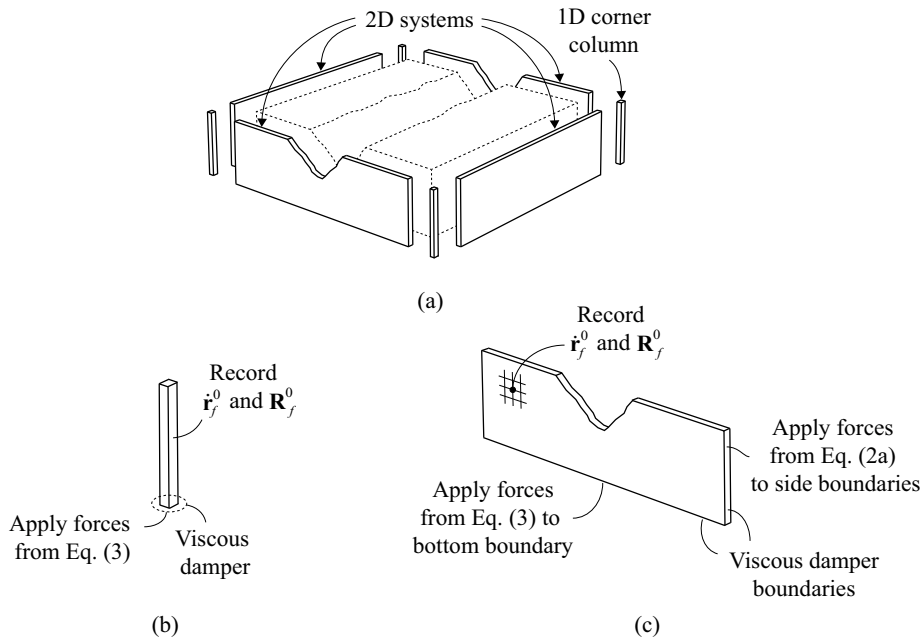

Figure 6: Computing $\mathbf{P}_f^0$ at side boundaries of foundation-rock domain: (a) free-field system with corresponding 1D corner columns and 2D systems; (b) example analysis of 1D corner column to compute $\dot{\mathbf{r}}_f^0$ and $\mathbf{R}_f^0$ at corners, (c) example analysis of 2D system to compute $\dot{\mathbf{r}}_f^0$ and $\mathbf{R}_f^0$ at the four side boundaries.

Implementation of this procedure (Box A2) means that eight auxiliary analyses are required for each of the three components of ground motion. The computational effort required for these linear dynamic analyses is minimal, and the procedure can be automated in a pre-processing script that is set up and executed before the nonlinear dynamic analysis of the dam–water–foundation rock system takes place. For example, we use MATLAB [40] to compute and store effective earthquake forces that are used with the FE code OPENSEES [41]; a similar methodology has been implemented by Saouma [42] with the FE code MERLIN [43].

This disadvantage of this approach is that substantial management and transfer of data is required for three-dimensional models, which may easily have tens of thousands of boundary nodes. The authors are currently developing a simplified form of the direct FE method that drastically reduces these requirements.

4.3. Forces at upstream boundary of fluid domain

The free-field hydrodynamic pressures $\mathbf{p}_r^0$ required to compute $\mathbf{P}_r^0$ at Γ_r are to be determined by dynamic analysis of the fluid in its free-field state: a fluid channel of uniform cross-section unbounded in the upstream direction (Fig. 5b). Because this system is uniform in the upstream direction, the analysis reduces to two dimensions. For cross-stream and vertical components of ground motion, the free-field pressures $\mathbf{p}_r^0$ on the boundary Γ_r are computed from analysis of the 2D fluid domain cross-section (Fig. 7); the stream component of ground motion will not generate any hydrodynamic pressures, thus implying $\mathbf{P}_r^0 = \mathbf{0}$. The procedure is summarized in step-by-step form in Box A3 in Appendix A.

Before closing this section we note that the forces $\mathbf{P}_r^0$ are associated with earthquake-induced hydrodynamic pressures caused by vertical and cross-stream excitation of the part of the fluid domain that has been eliminated upstream of Γ_r. These forces are required because of the system idealization (Fig.

1), where the earthquake excitation is implicitly assumed to extend along the entire length of the unbounded fluid channel.

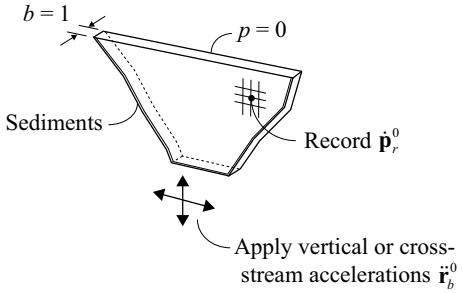

Figure 7: Computing $\mathbf{P}_r^0$ at upstream boundary of fluid domain: analysis of 2D fluid cross-section subjected to vertical and cross-stream excitation to compute $\dot{\mathbf{p}}_r^0$.

5. SUMMARY OF ANALYSIS PROCEDURE

The earthquake input for the three-dimensional dam–water–foundation rock system is the free-field ground acceleration $a_g^k(t)$, $k = x, y, z$, specified at a control point on the foundation-rock surface at the level of the dam abutments (Fig. 3c). This motion could for example be from an ensemble of recorded ground motions selected and scaled to "match" a target spectrum, or synthetic motions developed for an earthquake scenario.

Analysis of a 3D dam–water–foundation rock system by the direct FE method is organized in three major phases: initial static analysis, linear dynamic analyses of the free-field foundation-rock and fluid domains, and nonlinear dynamic analysis of the dam–water–foundation rock system [30].

Initial static analysis:

1. Develop a FE model for static analysis of the dam–foundation rock system with an appropriate material model for the dam concrete and an appropriate static model for the foundation rock.
2. Compute the response of this system to hydrostatic forces and the self-weight of the dam and foundation rock.
3. Record the static state of the dam and foundation rock, including displacements, stresses and strains, and reactions from the foundation rock at the boundary Γ_f.

Linear dynamic analysis of free-field foundation-rock and fluid domains:

4. Obtain the outcrop motion at the bottom boundary of the foundation-rock model by deconvolution of the surface ground motion $a_g(t)$.
5. Calculate the effective earthquake forces $\mathbf{P}_f^0$ at the bottom boundary of the foundation-rock domain using the procedure summarized in Box A1.
6. Compute the effective earthquake forces $\mathbf{P}_f^0$ at the side boundaries of the foundation-rock domain using the procedure summarized in Box A2.
7. Calculate the effective earthquake forces $\mathbf{P}_r^0$ at the upstream boundary of the fluid domain using the procedure summarized in Box A3.

Step 6 may be avoided if free-field boundary elements [37] are employed at the side boundaries of the truncated foundation-rock domain.

Nonlinear dynamic analysis of dam–water–foundation rock system:

8. Develop a FE model of the dam–water–foundation rock system with viscous-damper boundaries at the truncations of the semi-unbounded foundation-rock and fluid domains at Γ_f and Γ_r, respectively. Use solid elements for the dam and foundation rock, acoustic fluid elements for the water, interface elements at the dam–water and water–foundation rock interfaces, and surface elements for the sediments at the reservoir bottom and sides.
9. Calculate the response of this FE model subjected to effective earthquake forces $\mathbf{P}_f^0$ computed in Step 5 at the bottom foundation-rock boundary and in Step 6 at the side boundaries, $\mathbf{P}_r^0$ computed in Step 7 at the upstream fluid boundary, as well as self-weight, hydrostatic forces and static foundation-rock reactions at Γ_f. The static state of the dam (Step 3) is taken as the initial state in the nonlinear dynamic analysis.

6. NUMERICAL VALIDATION OF THE DIRECT FE METHOD

In this section, several examples are documented to validate the accuracy of the direct FE method, which was implemented with the FE program OPENSEES [41]. First, the ability of the method to reproduce free-field motions at the surface of a flat foundation box is documented. The free-field response of a uniform, semi-cylindrical canyon cut in a foundation halfspace is determined next and compared with classical solutions. Lastly, the dynamic response of Morrow Point Dam is computed and compared with results obtained from the substructure method.

6.1. Free-field motion at horizontal ground surface

The flat box model shown in Fig. 8a has a domain size and mesh density that is representative of an actual dam–water–foundation rock system, and viscous dampers employed at the bottom and side boundaries. A free-field control motion $a_g(t)$ is defined at the surface in the two horizontal and vertical directions by the S69E, S21W and vertical components, respectively, of the motion recorded at Taft Lincoln School Tunnel during the 1952 Kern County earthquake. Each component of ground motion is deconvolved, effective earthquake forces $\mathbf{P}_f^0$ are computed from the procedures summarized in Appendix A and applied to the bottom and side boundaries of the foundation domain, and the response of the system is computed.

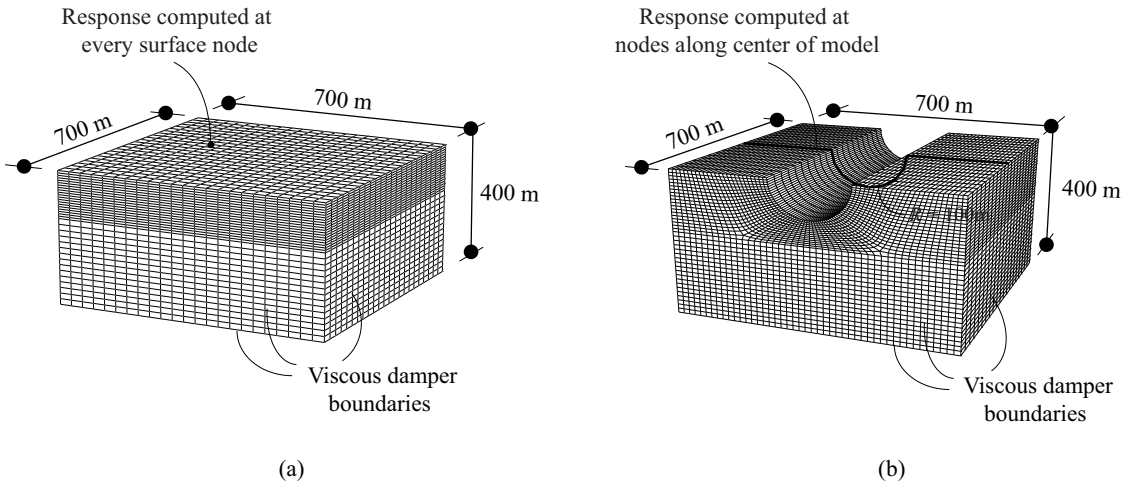

Figure 8: (a) FE model of flat foundation box, (b) FE model of semi-cylindrical canyon cut in halfspace.

The results presented in Fig. 9 show a near perfect match between the specified free-field control motion and the computed surface motions at every node at the surface of the flat box, thus demonstrating that the direct FE method is able to exactly reproduce free-field conditions for this simple system to within FE discretization error. This is achieved without using iterative procedures to adjust the amplitude and/or frequency content of the input motion, which is sometimes used by dam engineers to overcome deficiencies in their FE models.

6.2. Free-field motion at canyon surface

Next, we evaluate the ability of the direct FE method to accurately compute the free-field motion at the surface of a semi-cylindrical canyon; this is the motion that in turn will excite a dam supported in the canyon. Available analytical and numerical solutions for this classical problem [44,45] serve as the benchmark for the evaluation.

The semi-cylindrical canyon with radius R discretized as a FE system with viscous-damper boundaries (Fig. 8b) is subjected to effective earthquake forces $\mathbf{P}_f^0$ computed from the procedures summarized in Appendix A, but with the vertically incident seismic motion $\mathbf{r}_I^0$ specified as a plane wave of unit amplitude and frequency f. The forces $\mathbf{P}_f^0$ are applied to the bottom and side boundaries of the FE model, and the displacement response along the canyon and top surface of the foundation is computed. Results are presented for Poisson's ratio ν = 1/3 and different values of the dimensionless frequency $\eta = 2fR/V_s$, where V_s is the shear wave velocity of the foundation medium; η may be interpreted as the ratio of the canyon width to the wavelength of the incident waves. When plotted in this form, the results are independent of the actual material properties as long as the ratio R/V_s is maintained.

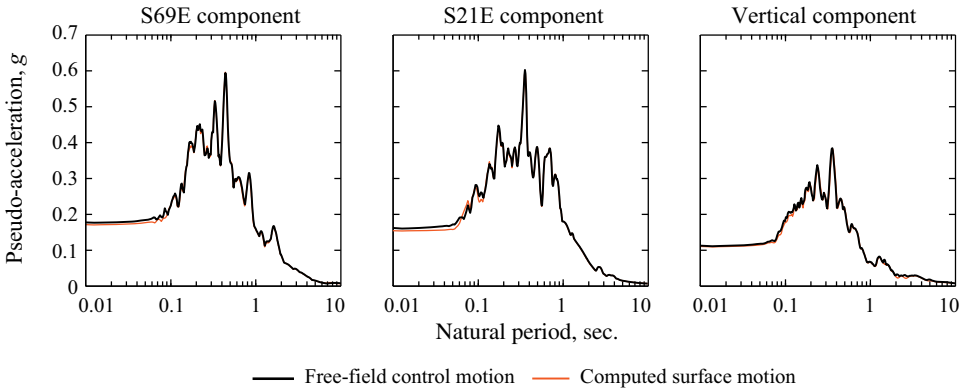

Figure 9: Comparison of 5% damped pseudo-acceleration response spectra for control motion and computed motion at nodes on flax box surface.

The displacement amplification, defined as the ratio of the Fourier transform of the computed displacements to the unit amplitude input motion, are presented in Fig. 10 for incident *SH*-, *SV*- and *P*-waves; these correspond to excitation in the canyon, cross-canyon and vertical directions, respectively. The results obtained by the direct FE method closely match the analytical results by Trifunac [44] for incident *SH*-waves, and the numerical results using boundary integral methods by Wong [45] for incident *SV*-waves and *P*-waves. The small discrepancies are due to the inability of the viscous damper boundaries to perfectly absorb all scattered and diffracted waves from the canyon. This is most prominent in the response to incident *SV*-waves and *P*-waves because these excitations generate surface waves that are not effectively absorbed by the viscous dampers; but even for these excitations, the discrepancies are small. The excellent agreement demonstrates the ability of the direct FE method to accurately predict free-field motions at the surface of a canyon.

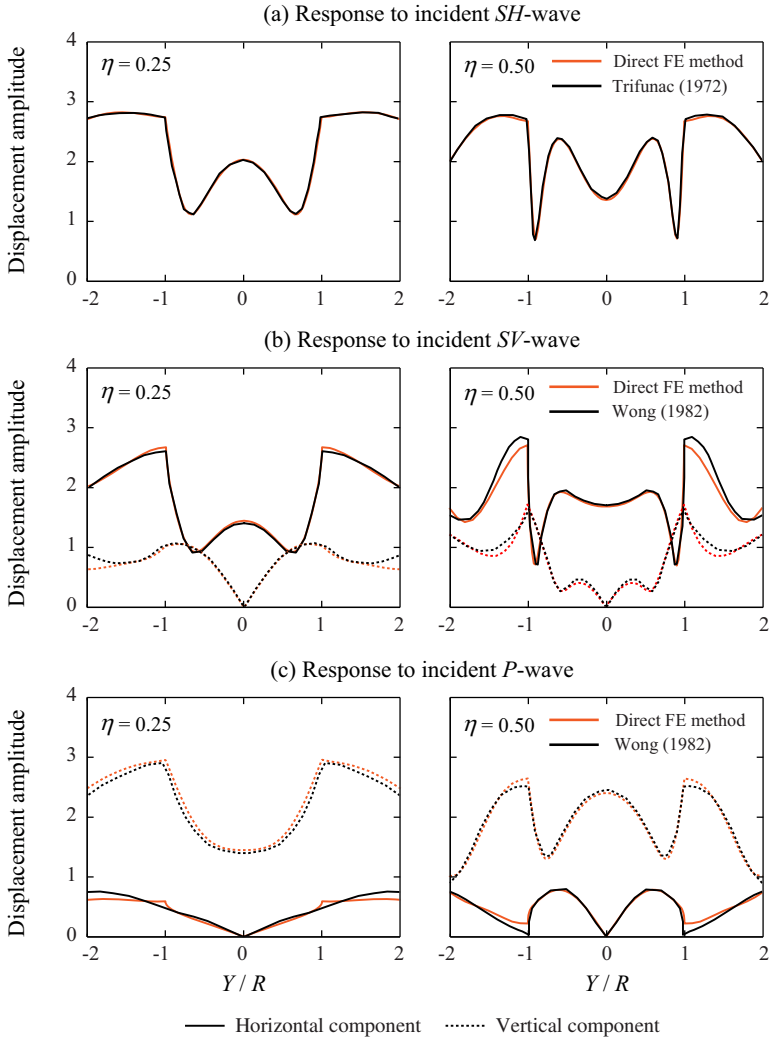

Figure 10: Displacement amplitudes at semi-cylindrical canyon computed by the direct FE method and compared with results by Trifunac [44] and Wong [45]. Responses to incident *SH*-, *SV*-, and *P*-waves are plotted against the dimensionless distance Y / R, where Y is the cross-canyon distance from the center of the canyon and R is the radius of the canyon.

6.3. Dynamic response of Morrow Point Dam

6.3.1. System analyzed

The ability of the direct FE method to accurately compute the dynamic response of concrete dams is evaluated numerically by analyzing Morrow Point Dam, a 142 m high, approximately symmetric, single centered arch dam located on the Gunnison River in Colorado. The material properties and damping values selected for the dam concrete and foundation rock are based on the results from forced vibration tests of the dam and subsequent numerical studies performed to match the experimental results [46,47]. The concrete and foundation rock is assumed to be homogeneous, isotropic and linearly elastic. The concrete has a modulus of elasticity E_s = 34.5 GPa, density ρ_s = 2403 kg/m^3, and Poisson's ratio ν_s = 0.20. The foundation rock has a modulus of elasticity E_f = 24.1 GPa (i.e. E_f / E_s = 0.70), density ρ_f =

2723 kg/m^3 and Poisson's ratio ν_f = 0.20. The impounded water has the same depth as the height of the dam, density ρ = 1000 kg/m^3, and pressure-wave velocity C = 1440 m/s. The reservoir-bottom reflection coefficient is chosen as α = 0.80.

Material damping in the dam and foundation rock is modeled in the direct FE method by Rayleigh damping with ζ_s = 1% and ζ_f = 2% viscous damping specified for the dam concrete and foundation rock, respectively, at two frequencies: f_1 = 5Hz, the fundamental resonance frequency of the dam on rigid rock, and at three times this frequency. The damping matrix for the complete system is then constructed using standard procedures for assembling damping matrices for two subdomains [48]. Determined by the half-power bandwidth method applied to the resonance curve, the overall damping in the combined dam–water–foundation rock system is 3-5% for the first few modes of vibration, consistent with the range of measured damping values [46].

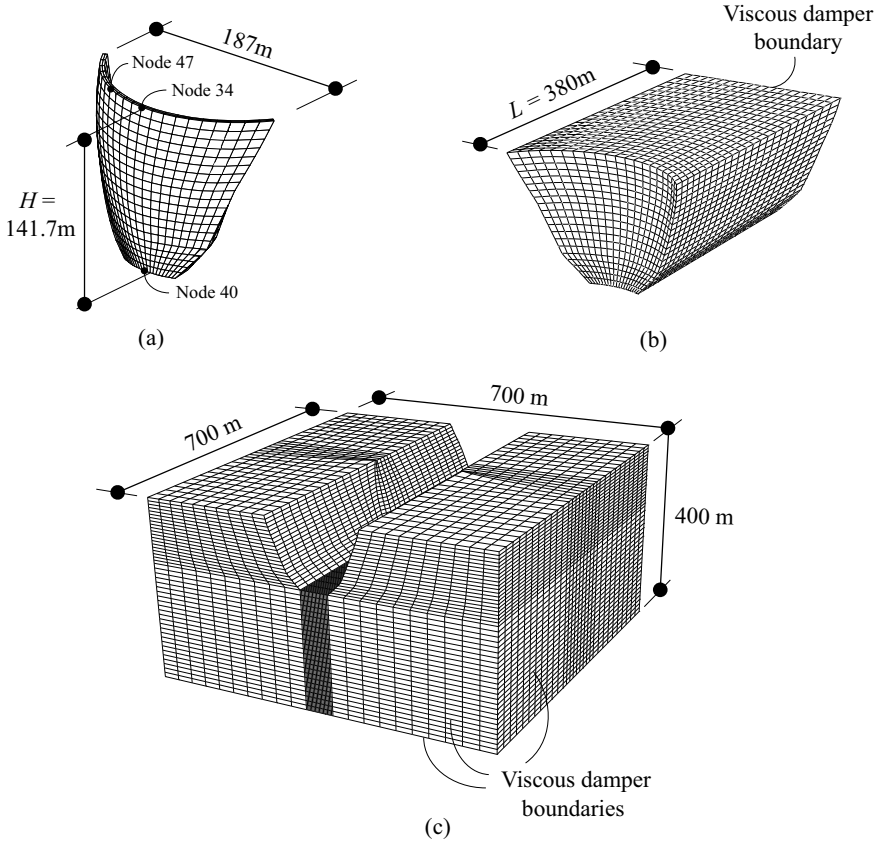

Figure 11: OpenSees FE model of Morrow Point Dam: (a) dam; (b) fluid domain; (c) foundation-rock domain.

The FE mesh shown in Fig. 11 is assembled using standard 8-node brick elements, with 800 full-integration solid elements for the dam, 42,000 reduced-integration solid elements for the foundation rock, and 9,200 acoustic fluid elements for the water in the reservoir. Interface elements couple accelerations with hydrodynamic pressures at the fluid-solid interfaces, surface elements at the bottom and sides of the reservoir model wave absorption due to sediments, and viscous dampers (dashpots) at the boundaries of the foundation-rock domain and at the upstream end of the fluid domain model the semi-unbounded extent of these domains. The combined FE model consists of approx. 63,000 elements and 150,000 DOFs, and its overall dimensions are 700m × 700m × 400m, corresponding to approx. 5H × 5H × 3H, where H is the height of the dam.

6.3.2. EACD3D-08 model for substructure method

The dynamic response of this FE model – computed by the direct FE method – will be compared with independent results obtained by frequency-domain analysis using the substructure method [14]. Analyzed using the computer program EACD3D-08 [15], wherein the foundation rock is treated as a semi-unbounded halfspace, the fluid domain as unbounded in the upstream direction, and the earthquake excitation is specified directly at the dam–canyon interface, this method avoids artificial model truncations and absorbing boundaries. The EACD3D-08 model, shown in Fig. 12, includes 800 solid elements for the dam, the FE mesh for the irregular part of the fluid domain, and the boundary element mesh at the dam–foundation rock interface.

Material damping in the substructure method is modeled by rate-independent, constant hysteretic damping defined by the damping factors η_s = 0.02 and η_f = 0.04 specified for the dam and foundation-rock separately; these correspond to viscous damping ratios of ζ_s = 1% and ζ_f = 2% at all frequencies of vibration. A numerical investigation confirmed that the damping in the direct FE method, as defined earlier, is sufficiently close to this rate-independent damping over the frequency range of interest [30]. Because EACD3D-08 does not consider water–foundation rock interaction, this is also excluded in the direct FE method to ensure a meaningful comparison.

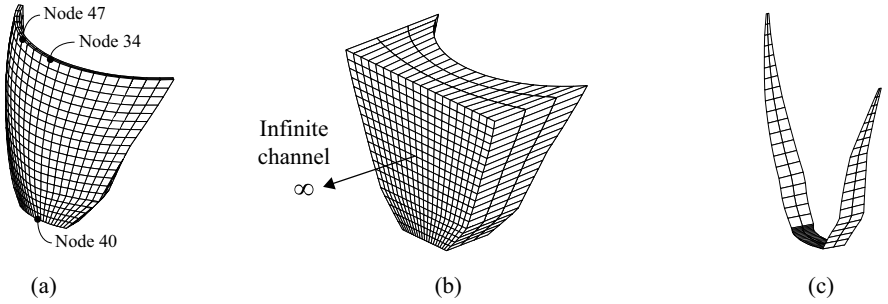

Figure 12: EACD3D-08 model for Morrow Point Dam: (a) FE model for dam, (b) FE model for semi-unbounded fluid domain, (c) boundary element mesh for foundation-rock domain discretized at the dam–canyon interface.

6.3.3. Frequency response functions for dam response

Results for the dam response are presented in the form of dimensionless frequency response functions that represent the amplitude of radial acceleration at the crest of the dam† due to unit harmonic free-field motion. These functions are determined in the direct FE method from time-domain analysis of the FE model (Fig. 11) subjected to effective earthquake forces computed from the procedures summarized in Appendix A at the bottom and side boundaries of the foundation rock and at the upstream fluid boundary. The free-field control motion, $a_g(t)$, is specified at the control point on the foundation-rock surface as a long sequence of unit harmonics with gradually increasing frequency; further details of this procedure are available in [30].

Implemented in the frequency domain, the substructure method directly provides frequency response functions; however, the earthquake excitation is here defined by the free-field motion at the dam–canyon interface. To determine this motion consistent with the specified control motion $a_g(t)$, we implement a direct FE analysis of the foundation-rock domain without the dam or impounded water (Fig. 13) subjected to the same boundary forces $\mathbf{P}_f^0$ as described in the preceding paragraph. The motion

† The actual location at the dam crest is selected at node 34 – the center node – for upstream and vertical ground motions, and at node 47 for cross-stream motion.

recorded at the dam–canyon interface is then used as the spatially varying input excitation to the EACD3D-08 analysis.

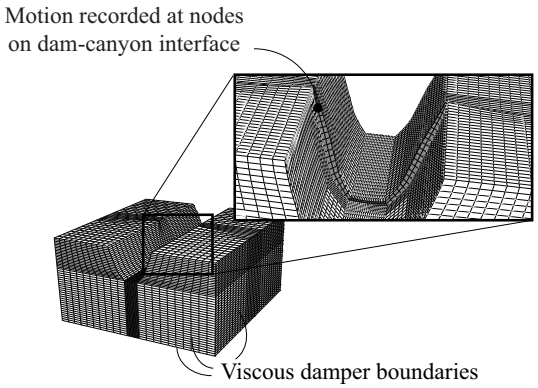

Figure 13: FE model of foundation-rock domain to compute
free-field motion at dam–canyon interface used as input to EACD3D-08 analysis.

Frequency response functions obtained by the direct FE and substructure methods for the dam on flexible foundation rock are compared for two cases: empty reservoir and full reservoir in Figs. 14 and 15, respectively. Additional validation examples for the dam–water–foundation rock system covering a wide range of conditions are available in [30]. Results for a full reservoir are presented here only for the stream component of ground motion, because limitations in the EACD3D-08 computer program does not allow for a meaningful comparison with the direct FE method for cross-stream and vertical ground motions.

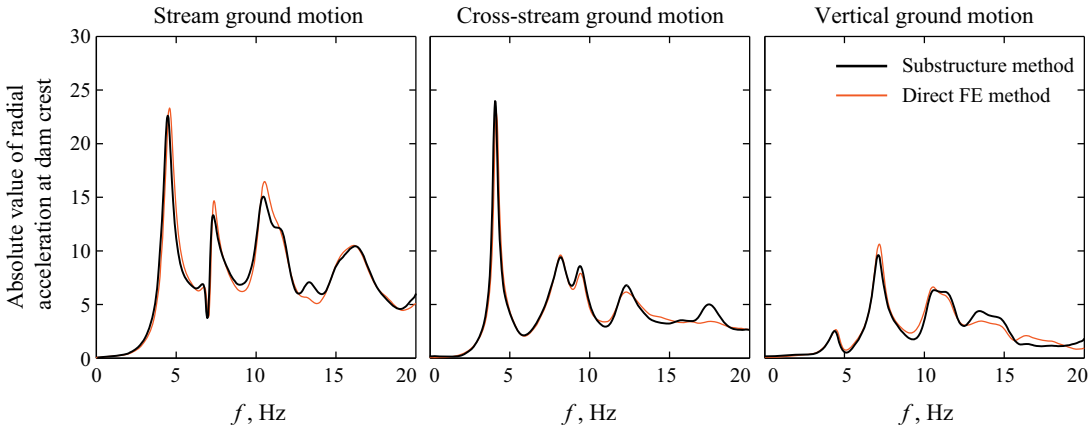

Figure 14: Frequency response functions for the amplitude of radial acceleration at the crest of Morrow Point dam including dam–foundation rock interaction (empty reservoir) subjected to stream, cross-stream and vertical ground motions. Results are computed by direct FE and substructure methods.

The response results obtained by the direct FE method are very close to those from the substructure method. The small discrepancies near some of the resonant peaks (Fig. 14), and at frequencies higher than 15 Hz (Fig. 15), are primarily caused by reflections from the viscous-damper boundaries, which are incapable of perfectly absorbing all scattered waves. Such errors will generally decrease with larger domain sizes.

The good agreement demonstrates the ability of the direct FE method to model the factors important for earthquake analysis of arch dams: dam–water–foundation rock interaction including water compressibility and wave absorption at the reservoir boundaries, radiation damping in the semi-unbounded foundation-rock and fluid domains, and the earthquake excitation specified by a control motion at the surface of the foundation-rock domain.

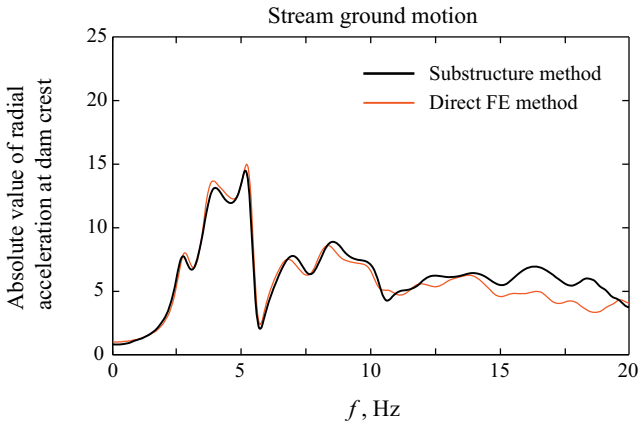

Figure 15: Frequency response functions for the amplitude of radial acceleration at the crest of Morrow Point dam including dam–water–foundation rock interaction (full reservoir) subjected to stream ground motion. Results are computed by direct FE and substructure methods.

6.3.4. Response to earthquake excitation

The FE system in Fig 11 is analyzed with the free-field control motion in the stream direction, $a_g^x(t)$, defined by the S69E component of the Taft ground motion. The radial accelerations and displacements at the crest of the dam relative to the base of the dam (node 40) are presented in Fig. 16, and envelope values of maximum tensile arch and cantilever stresses on the upstream face of the dam in Fig. 17. The results computed by the direct FE method closely match those from the substructure method: the displacements and accelerations at the crest show a near perfect match, and the envelope stress values are also close. The slight discrepancies in the stress contour plots were found to be caused by differences between the FE stress recovery algorithms in the two computer programs.

The effectiveness of the direct FE method with viscous-damper boundaries is apparent from the fact that these excellent results (Figs. 14-17) are achieved even with relatively moderate domain sizes: the overall dimensions of the FE model are approx. $5H \times 5H \times 3H$, where H is the height of the dam. In passing, we note that larger domains were required to ensure similar levels of accuracy for two-dimensional analysis of gravity dams [24].

The direct FE analyses were implemented in OPENSEES on a laptop computer (without parallel processing capabilities) using simple MATLAB scripts to perform the data management for computing and applying effective earthquake forces. The CPU-time required in determining the dynamic response of the FE model in Fig. 12 with roughly 150,000 DOFs was 68 min for 2000 time-steps; approximately 13 min were required for the auxiliary analyses to set up the effective earthquake forces, and 55 min for the linear dynamic analysis of the dam–water–foundation rock system. The computational effort required to determine the effective earthquake forces for the system is small compared to the time required for dynamic analysis of the overall system. Clearly, it will become negligible compared to the CPU-time required to perform a more sophisticated nonlinear dynamic analysis of such systems.

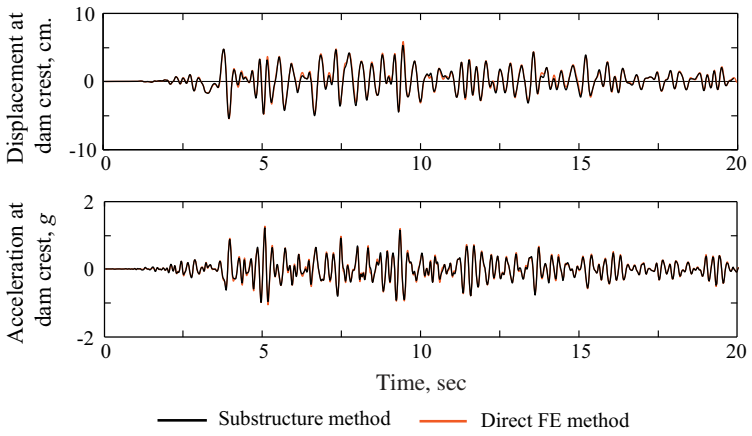

Figure 16: Radial displacements and accelerations at the crest of Morrow Point Dam including dam–water–foundation rock interaction subjected to S69E component of Taft ground motion applied in the stream direction. Results are computed by direct FE and substructure methods.

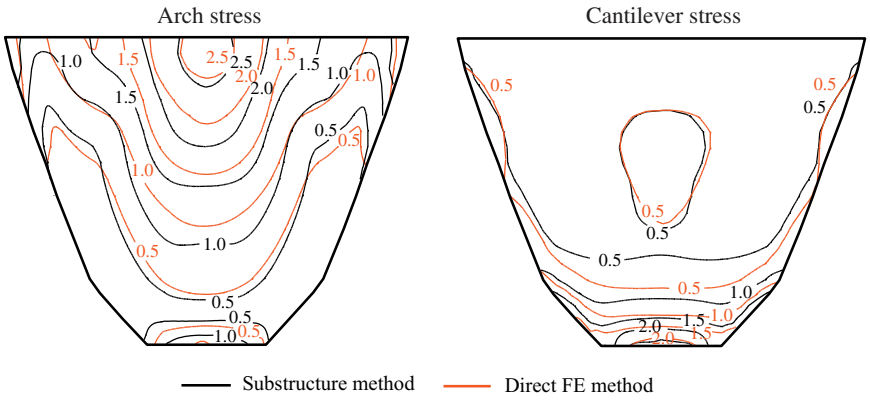

Figure 17: Envelope values of maximum tensile stresses, in MPa, on the upstream face of Morrow Point Dam including dam–water–foundation rock interaction subjected to S69E component of Taft ground motion applied in the stream direction; static stresses are excluded. Results are computed by direct FE and substructure methods.

7. CONCLUSIONS

The direct FE method with viscous-damper boundaries that was recently presented for nonlinear earthquake analysis of two-dimensional dam–water–foundation rock systems [24] has been generalized to three-dimensional systems. This analysis procedure considers all the factors important in the earthquake response of arch dams: dam–water interaction including water compressibility and wave absorption at the reservoir boundaries; dam–foundation rock interaction including mass, stiffness and damping in the rock; radiation damping due to the semi-unbounded sizes of the foundation-rock and fluid domains; spatial variation of the ground motions around the dam–canyon interface; and nonlinear behavior in the dam and adjacent parts of the foundation-rock and fluid domains.

The seismic input to the procedure is specified by a free-field ground motion at a control point on the surface of the foundation rock. Deconvolution of this control motion provides the motion at the bottom boundary of the foundation-rock domain. Then, effective earthquake forces are computed from a

set of 1D and 2D analyses and applied to the boundaries of the FE model. Each of these analyses is simple, requires very little computational effort and can be implemented without modifying the FE source code, the main challenge is the management and transfer of large amounts of data.

Several examples have been documented to validate the accuracy of the direct FE method applied to three-dimensional problems. One of these examples compares the dynamic response of Morrow Point Dam computed by the direct FE method with independent benchmark solutions obtained by the substructure method. The close agreement demonstrates that (i) the effects of dam–water–foundation rock interaction are accurately modeled, (ii) the bounded foundation-rock and fluid models with viscous-damper boundaries are able to simulate the semi-unbounded extent of these domains, and (iii) the earthquake excitation is appropriately defined by specifying – at the boundaries of the FE model – effective earthquake forces determined from a surface control motion.

ACKNOWLEDGEMENTS

The authors are grateful to Dr. Frank McKenna for his advice and support on implementing large three-dimensional fluid-soil-structure interacting models in OpenSees. The first author would also like to thank Professors Svein Remseth and Amir Kaynia at the Norwegian University of Science and Technology (NTNU) for their encouragement and support.

REFERENCES

1. Chopra AK. Earthquake analysis of arch dams: Factors to be considered. *Journal of Structural Engineering* 2012; **138**(2): 205–214. DOI: 10.1061/(ASCE)ST.1943-541X.0000431.
2. Fok KL, Chopra AK. Hydrodynamic and foundation flexibility effects in earthquake response of arch dams. *Journal of Structural Engineering* 1986; **112**(8): 1810–1828. DOI: 10.1061/(ASCE)0733-9445(1986)112:8(1810).
3. Tan H, Chopra AK. Dam-foundation rock interaction effects in earthquake response of arch dams. *Journal of Structural Engineering* 1996; **122**(5): 528–538. DOI: 10.1061/(ASCE)0733-9445(1996)122:5(528).
4. Maeso O, Domínguez J. Earthquake analysis of arch dams. I: dam-foundation interaction. *Journal of Engineering Mechanics* 1993; **119**(3): 496–512. DOI: 10.1061/(ASCE)0733-9399(1993)119:3(496).
5. Zhang CH, Pan JW, Wang JT. Influence of seismic input mechanisms and radiation damping on arch dam response. *Soil Dynamics and Earthquake Engineering* 2009; **29**(9): 1282–1293. DOI: 10.1016/j.soildyn.2009.03.003.
6. Alves SW, Hall JF. Generation of spatially nonuniform ground motion for nonlinear analysis of a concrete arch dam. *Earthquake Engineering & Structural Dynamics* 2006; **35**(11): 1339–1357. DOI: 10.1002/eqe.576.
7. Maeso O, Aznárez JJ, Domínguez J. Effects of space distribution of excitation on seismic response of arch dams. *Journal of Engineering Mechanics* 2002; **128**(7): 759–768. DOI: 10.1061/(ASCE)0733-9399(2002)128:7(759).
8. Niwa A, Clough RW. Non-linear seismic response of arch dams. *Earthquake Engineering & Structural Dynamics* 1982; **10**(2): 267–281. DOI: 10.1002/eqe.4290100208.
9. Bhattacharjee SS, Léger P. Seismic cracking and energy dissipation in concrete gravity dams. *Earthquake Engineering & Structural Dynamics* 1993; **22**(11): 991–1007. DOI: 10.1002/eqe.4290221106.
10. Fenves G, Mojtahedi S, Reimer RB. Effect of contraction joints on earthquake response of an arch dam. *Journal of Structural Engineering* 1992; **118**(4): 1039–1055. DOI: 10.1061/(ASCE)0733-9445(1992)118:4(1039).
11. Lemos J V. Discrete element analysis of dam foundations. *Distinct Element Modelling in Geomechanics*, Rotterdam: Balkema; 1999.
12. Pan JW, Zhang CH, Xu Y, Jin F. A comparative study of the different procedures for seismic cracking analysis of concrete dams. *Soil Dynamics and Earthquake Engineering* 2011; **31**(11): 1594–1606. DOI:

10.1016/j.soildyn.2011.06.011.
13. Tan H, Chopra AK. Earthquake analysis of arch dams including dam-water-foundation rock interaction. *Earthquake Engineering & Structural Dynamics* 1995; **24**(11): 1453–1474. DOI: 10.1002/eqe.4290241104.
14. Wang JT, Chopra AK. Linear analysis of concrete arch dams including dam-water-foundation rock interaction considering spatially varying ground motions. *Earthquake Engineering & Structural Dynamics* 2010; **39**(7): 731–750. DOI: 10.1002/eqe.968.
15. Wang JT, Chopra AK. EACD-3D-2008: A computer program for three-dimensional earthquake analysis of concrete dams considering spatially-varying ground motion. *Report No. UCB/EERC-2008/04*, Earthquake Engineering Research Center, Univ. of California, Berkeley: 2008.
16. Kellezi L. Local transmitting boundaries for transient elastic analysis. *Soil Dynamics and Earthquake Engineering* 2000; **19**(7): 533–547. DOI: 10.1016/S0267-7261(00)00029-4.
17. Wolf JP. *Soil-Structure Interaction in Time Domain*. Englewood Cliffs, NJ: Prentice Hall; 1988.
18. Zienkiewicz OC, Bicanic N, Shen FQ. Earthquake input definition and the transmitting boundary conditions. *Advances in Computational Nonlinear Mechanics*, Springer; 1989.
19. Bielak J, Christiano P. On the effective seismic input for non-linear soil-structure interaction systems. *Earthquake Engineering & Structural Dynamics* 1984; **12**(3): 107–119. DOI: 10.1002/eqe.4290120108.
20. Bielak J, Loukakis K, Hisada Y, Yoshimura C. Domain reduction method for three-dimensional earthquake modeling in localized regions, Part I: Theory. *Bulletin of the Seismological Society of America* 2003; **93**(2): 817–824. DOI: 10.1785/0120010251.
21. Basu U. Perfectly matched layers for acoustic and elastic waves: Theory, finite-element implementation and application to earthquake analysis of dam-water-foundation rock systems. PhD thesis, University of California, Berkeley, 2004.
22. Basu U, Chopra AK. Perfectly matched layers for transient elastodynamics of unbounded domains. *International Journal for Numerical Methods in Engineering* 2004; **59**(8): 1039–1074. DOI: 10.1002/nme.896.
23. Hallquist JO. LS-DYNA keyword user's manual, Livermore Software Technology Corporation 2016.
24. Løkke A, Chopra AK. Direct finite element method for nonlinear analysis of semi-unbounded dam-water-foundation rock systems. *Earthquake Engineering & Structural Dynamics* 2017; **46**(8): 1267–1285. DOI: 10.1002/eqe.2855.
25. Lysmer J, Kuhlemeyer RL. Finite dynamic model for infinite media. *Journal of the Engineering Mechanics Division* 1969; **95**(4): 859–878.
26. Bielak J, Graves RW, Olsen KB, Taborda R, Ramirez-Guzman L, Day SM, *et al.* The ShakeOut earthquake scenario: verification of three simulation sets. *Geophysical Journal International* 2010; **180**(1): 375–404. DOI: 10.1111/j.1365-246X.2009.04417.x.
27. He C, Wang JT, Zhang CH. Nonlinear spectral-element method for 3D seismic-wave propagation. *Bulletin of the Seismological Society of America* 2016; **106**(3): 1074–1087. DOI: 10.1785/0120150341.
28. García F, Aznárez JJ, Padrón LA, Maeso O. Relevance of the incidence angle of the seismic waves on the dynamic response of arch dams. *Soil Dynamics and Earthquake Engineering* 2016; **90**: 442–453. DOI: 10.1002/eqe.4290201104.
29. Kwong NS, Chopra AK, McGuire RK. A framework for the evaluation of ground motion selection and modification procedures. *Earthquake Engineering & Structural Dynamics* 2015; **44**(5): 795–815. DOI: 10.1002/eqe.2502.
30. Løkke A, Chopra AK. A direct finite element method for nonlinear earthquake analysis of two-and three-dimensional semi-unbounded dam-water-foundation rock systems. *Report UCB/EERC (in preparation)*, Pacific Earthquake Engineering Research Center, Univ. of California, Berkeley, CA: .
31. Zienkiewicz OC, Bettess P. Fluid-structure dynamic interaction and wave forces. An introduction to numerical treatment. *International Journal for Numerical Methods in Engineering* 1978; **13**(1): 1–16. DOI: 10.1002/nme.1620130102.
32. Fenves G, Chopra AK. Effects of reservoir bottom absorption on earthquake response of concrete gravity dams. *Earthquake Engineering & Structural Dynamics* 1983; **11**(6): 809–829. DOI: 10.1002/eqe.4290110607.
33. Schnabel PB, Lysmer J, Seed HB. SHAKE: A computer program for earthquake response analysis of horizontally layered sites. *Report No. UCB/EERC-72/12*, Earthquake Engineering Research Center, Univ. of California, Berkeley: 1972.

34. Hashash YMA, Groholski DR, Phillips CA, Park D, Musgrove M. DEEPSOIL user manual and tutorial. Version 5.0, University of Illinois, Urbana, IL, USA 2011.
35. Mejia LH, Dawson EM. Earthquake deconvolution for FLAC. *Proc. of the 4th International FLAC Symposium on Numerical Modeling in Geomechanics*, 2006.
36. Robbe E, Kashiwayanagi M, Yamane Y. Seismic analyses of concrete dam, comparison between finite-element analyses and seismic records. *Proc. for 16th World Conference on Earthquake Engineering*, Santiago, Chile: 2017.
37. Nielsen AH. Towards a complete framework for seismic analysis in Abaqus. *Proceedings of the Institution of Civil Engineers - Engineering and Computational Mechanics* 2014; **167**(1): 3–12. DOI: 10.1680/eacm.12.00004.
38. Brinkgreve RBJ, Engin E, Swolfs WM. Plaxis Reference Manual 2016. *Plaxis BV, The Netherlands*.
39. Itasca Consulting Group Inc. FLAC3D - Fast Lagrangian Analysis of Continua in Three-Dimensions, Ver. 5.0., Minneapolis, USA 2012.
40. The MathWorks Inc. MATLAB user's guide (R2012a). Natick, MA, USA 2012.
41. McKenna F. OpenSees: A framework for earthquake engineering simulation. *Computing in Science and Engineering* 2011; **13**(4): 58–66. DOI: 10.1109/MCSE.2011.66.
42. Saouma V, Miura F, Lebon G, Yagome Y. A simplified 3D model for soil-structure interaction with radiation damping and free field input. *Bulletin of Earthquake Engineering* 2011; **9**(5): 1387–1402. DOI: 10.1007/s10518-011-9261-7.
43. Saouma V, Cervenka J, Reich R. Merlin finite element user's manual, Univ. of Colorado, Boulder 2013.
44. Trifunac MD. Scattering of plane SH waves by a semi-cylindrical canyon. *Earthquake Engineering & Structural Dynamics* 1972; **1**(3): 267–281. DOI: 10.1002/eqe.4290010307.
45. Wong HL. Effect of surface topography on the diffraction of P, SV, and Rayleigh waves. *Bulletin of the Seismological Society of America* 1982; **72**(4): 1167–1183.
46. Duron ZH, Hall JF. Experimental and finite element studies of the forced vibration response of Morrow Point Dam. *Earthquake Engineering & Structural Dynamics* 1988; **16**(7): 1021–1039.
47. Nuss L. Comparison of EACD3D96 computed response to shaker tests on Morrow Point Dam. *Technical Memorandum No. MP-D8110-IE-2001-2*, Denver, CO: US Bureau of Reclamation; 2001.
48. Chopra AK. *Dynamics of Structures: Theory and Applications to Earthquake Engineering*. Upper Saddle River, NJ: Prentice Hall; 2012.
49. Zienkiewicz OC, Paul DK, Hinton E. Cavitation in fluid-structure response (with particular reference to dams under earthquake loading). *Earthquake Engineering & Structural Dynamics* 1983; **11**(4): 463–481. DOI: 10.1002/eqe.4290110403.

APPENDIX A

Presented in this appendix are step-by-step procedures for computing effective earthquake forces $\mathbf{P}_f^0$ at the bottom and side boundaries of the foundation-rock domain and $\mathbf{P}_r^0$ at the upstream boundary of the fluid domain. Additional details regarding the computational procedures can be found in [30].

Box A1: Step-by-step procedure for computing $\mathbf{P}_f^0$ at bottom boundary of foundation-rock domain.

1. Determine the *outcrop motion* at the bottom foundation–rock boundary by one-dimensional deconvolution of each component of the surface control motion $a_g^k(t)$; $k = x, y, z$.
2. Compute the incident motion $\mathbf{r}_I^0$ as one-half of the outcrop motion at the bottom boundary determined in Step 1.
3. Calculate the effective earthquake forces $\mathbf{P}_f^0$ at the bottom boundary from Eq. (3) using $\mathbf{r}_I^0$ from Step 2.

Box A2: Step-by-step procedure for computing $\mathbf{P}_f^0$ at side boundaries of foundation-rock domain.

Analysis of four 1D corner columns (Fig. 6b)

1. Develop FE models for each of the four 1D corner columns for the foundation rock that have the same mesh density as the corners of the main FE model.
2. For each component of ground motion, $k = x, y, z$, add a viscous damper at the base in the *k*-direction and constrain DOFs in other directions to permit only shear ($k = x, y$) or axial ($k = z$) deformation of the 1D column.
3. Apply effective earthquake forces (Eq. 3) to the base in *k*-direction and compute $\dot{\mathbf{r}}_f^0$ and $\mathbf{R}_f^0$ at every node along the height.

Analysis of four 2D systems (Fig. 6c)

4. Develop FE models for each of the four 2D systems for the foundation rock, with the same mesh density as the side boundaries of the main FE model.
5. For each component of ground motion, $k = x, y, z$, add viscous dampers at the bottom and side boundaries and constrain DOFs at the faces to model "infinite length" conditions in the direction normal to the boundary (e.g., if the *x*-axis is normal to the boundary, two nodes with the same *y*-, and *z*-coordinates should be constrained to move identically).
6. Apply effective earthquake forces from Eq. (3) to the bottom boundary and from Eq. (2a) to the side boundaries using $\dot{\mathbf{r}}_f^0$ and $\mathbf{R}_f^0$ from the 1D analyses in Step 3, and compute $\dot{\mathbf{r}}_f^0$ and $\mathbf{R}_f^0$ at every node in the 2D system.

Computing effective earthquake forces

7. Compute the effective earthquake forces $\mathbf{P}_f^0$ at every node on the four side boundaries of the foundation-rock domain from Eq. (2a) using $\dot{\mathbf{r}}_f^0$ and $\mathbf{R}_f^0$ from Step 6.

Box A3: Step-by-step procedure for computing $\mathbf{P}_r^0$ at upstream boundary of fluid domain.

Analysis of two-dimensional fluid section (Fig. 7)

1. Develop a FE model of the 2D fluid cross-section with the same mesh density as the main model at the upstream fluid boundary Γ_r, add surface elements at the reservoir bottom and sides to model sediments.
2. For cross-stream and vertical components of ground motion, $k = y, z$, calculate $\dot{\mathbf{p}}_r^0$ at every node by analyzing the 2D model subjected to accelerations $\ddot{\mathbf{r}}_b^0$ at the reservoir bottom and sides, where $\ddot{\mathbf{r}}_b^0$ is the (spatially varying) foundation-rock accelerations at the intersection $\Gamma_b \cap \Gamma_r$; this can be extracted from the relevant 2D analysis described in Box A2.

Computing effective earthquake forces

3. Compute the effective earthquake forces $\mathbf{P}_r^0$ for every node at the fluid boundary from Eq. (2b) using $\dot{\mathbf{p}}_r^0$ from Step 2.